PHYSICAL REVIEW B

CONDENSED MATTER

THIRD SERIES, VOLUME 39, NUMBER 6 15 FEBRUARY 1989-II

Shadow-cone-enhanced secondary-ion mass-spectrometry studies of Ag{110}

Che-Chen Chang* and Nicholas Winograd

Department of Chemistry, The Pennsylvania State University, 152 Davey Laboratory, University Park, Pennsylvania 16802

(Received 31 August 1988)

The yield of particles ejected due to keV ion bombardment of Ag{110} has been observed to depend strongly on the angle of incidence of the primary ion beam. The desorption angles of these particles are found to reflect both the crystallographic and chemical structure of the surface. Molecular dynamics calculations indicate that the desorption yield of all particles is significantly enhanced when the shadow cone of the incident beam of particles created by a surface atom intersects adjacent surface atoms. These angles may be accurately calculated by use of a full three-dimensional trajectory calculation of the scattering or by simple computation of the angle of this intersection using a two-body Molière interaction potential function. With this approach it is possible to assign all of the angular anisotropies observed from secondary ions ejected from Ag{110}. Moreover, a detailed analysis suggests that the topmost atomic layer is relaxed inward by (7.8±2.5)% and that the spacing between the first and third layer is contracted by (4.1±2.1)% relative to the bulk spacings. These results are in excellent agreement with recent Rutherford backscattering experiments. A number of new possible applications of this technique to the analysis of chemisorbed overlayers is also discussed.

I. INTRODUCTION

There has been considerable recent interest in employing energetic ion beams in surface-structure characterizations. Using MeV ion backscattering methods, for example, it has been possible to determine atomic locations with high precision and to unravel rather complex surface reconstructions.[1-3] These determinations are possible since the incident ion may be channeled or blocked by the ordered array of near-surface atoms such that atomic locations may be straightforwardly deduced from the angular dependence of the scattered-ion intensity. At lower energies, similar studies are possible by examining the intensity of ions backscattered through nearly 180°.[4] Here the scattered-ion intensity is sensitive to the incident condition where the shadow cone of a surface atom intersects an adjacent surface atom. This experimental configuration, termed impact-collision ion-scattering spectrometry (ICISS), has proven important in evaluating semiconductor surface rearrangements,[5] in determining the structure of chemisorbed layers,[6] and in measuring surface Debye-Waller factors.[7] Finally, by examining the angular distributions of ion-induced desorbed particles, the bonding geometry of chemisorbed atoms and molecules may be determined using rather straightforward channeling and blocking arguments.[8,9]

It is possible to combine a number of the above features to develop a new approach to ion-beam surface-structure studies. In our experiment, we take advantage of the fact that the shadow cone created by collision of the primary ion with a surface atom focuses flux to specific surface coordinates. When the tail of this shadow cone strikes a surface or near-surface atom, the desorption yield should dramatically increase. With knowledge of the angle of incidence of the primary beam and the shadow-cone shape, it is then feasible to determine surface geometries using a strategy similar to that developed for ICISS.

In this work, we examine the basic concepts behind this unique scheme using the clean Ag{110} surface as a model. A number of theoretical approaches are examined to check our proposed explanation of observed angular anisotropies. These range from full three-dimensional computer simulations of the ion-impact event to very simple approaches using only two-body interaction potentials to describe the shadow-cone shapes. The results of these calculations yield predictions which are in excellent agreement with previous Rutherford backscattering studies of the Ag{110} surface reconstruction.[2,3] Our studies suggest that the truncated top layer of the bulk crystal is relaxed inward by (7.8±2.5)% and that the spacing between the first and third layer is contracted by (4.1±2.1)% relative to bulk values. The implications of this new experimental scheme for determining the structure of adsorbed layers are discussed. The possible advantages and disadvantages of this approach over ICISS are also considered.

II. EXPERIMENTAL ASPECTS

The ultrahigh-vacuum (UHV) chamber equipped with low-energy electron diffraction (LEED), Auger-electron spectroscopy (AES), a Riber AQX 156 quadrupole mass filter, and a modified Riber C150 noble-gas-ion gun has been described in detail previously.[10] The base pressure of the cyropumped chamber is $\sim 1\times 10^{-10}$ Torr. The Ag crystal was cut and oriented to within 0.5° of the desired {110} face and mechanically polished to optical quality before being mounted on the copper sample holder. Cycles of Ar^+-ion rastering (2 keV, 0.5 $\mu A\,cm^{-2}$) followed by annealing at 800–850 K were repeated *in situ* until no contamination could be detected by AES or secondary-ion mass spectrometry (SIMS). After this cleaning procedure, a sharp (1×1) LEED pattern characteristic of a clean surface is obtained.

Except as otherwise noted, the angular distributions of the secondary ions in this work are determined by measuring the intensity of the ions desorbed from the surface as a function of the angle of incidence θ_i. The definitions of the angles employed in this configuration are shown in Fig. 1. We shall refer to the incident angle associated with a local maximum in secondary-ion intensity as θ_{ic}. To obtain these measurements a crystal manipulator was constructed that permits independent translation along three Cartesian axes and independent rotation around two perpendicular axes parallel and perpendicular to the sample surface. The value of θ_i was controlled with an accuracy of better than ±0.5°. Typical polar angle distributions were performed with a 2–4-keV primary beam of Ar^+ ions at a current of less than 10 nA and with a beam cross section of less than 2 mm^2. The data collection time per spectrum was ~4 min. The sample was rastered and annealed after ~30 min of data collection in order to ensure that the surface was free of defects created by the ion bombardment process. During each polar scan, the angle β between the ion gun and the detector was fixed at a certain angle while θ_i was varied. The detected secondary ions ejected in the plane of the incident beam were energy selected using a 90° electrostatic energy analyzer operated in a low energy resolution mode.

III. DESCRIPTION OF THE CALCULATIONS

Several theoretical descriptions of the desorption process were attempted in order to elucidate the dynamics of the ion-solid event and to evaluate the level of calculation required for possible bond-length determinations. To establish the importance of shadow cones in the desorption process, a number of two-dimensional computer simulations were performed to calculate incident ion trajectories in the plane of incidence. Full three-dimensional calculations were performed using previously developed methods[11,12] to calculate the desorption yield of substrate atoms as a function of angle of incidence.

The same basic form of the potential function was employed for all of the computer simulations reported here. A pairwise-additive Thomas-Fermi Moliére potential was used to describe the interaction between the Ar primary particle and the Ag surface atom.[8,13] It is not completely clear at this stage how to pick an accurate scaling factor for the Firsov screening length. Although values near 0.8 appear to be appropriate for collisions between a light particle and a heavy particle,[14,15] few reports are available to describe collisions of the type examined here. On the other hand, systematic studies on the scattering potential for particles of different masses reflected from surfaces indicate that the scaling factor increases slightly with the sum of the incident ion and target mass.[16–18] For example, a factor of 1.0 was found to be adequate in describing K^+ scattering from Mo{100} surface.[16] Attempts to parametrize experimental results of gas-surface scattering yield a value of 1.02–1.04 for Ar scattering from a Ag surface.[18] In the model two- and three-dimensional calculations employed to check the validity of our basic hypotheses, we have arbitrarily chosen a value of 1.0 for this scaling factor. When attempting a detailed analysis of the experimental results, however, a

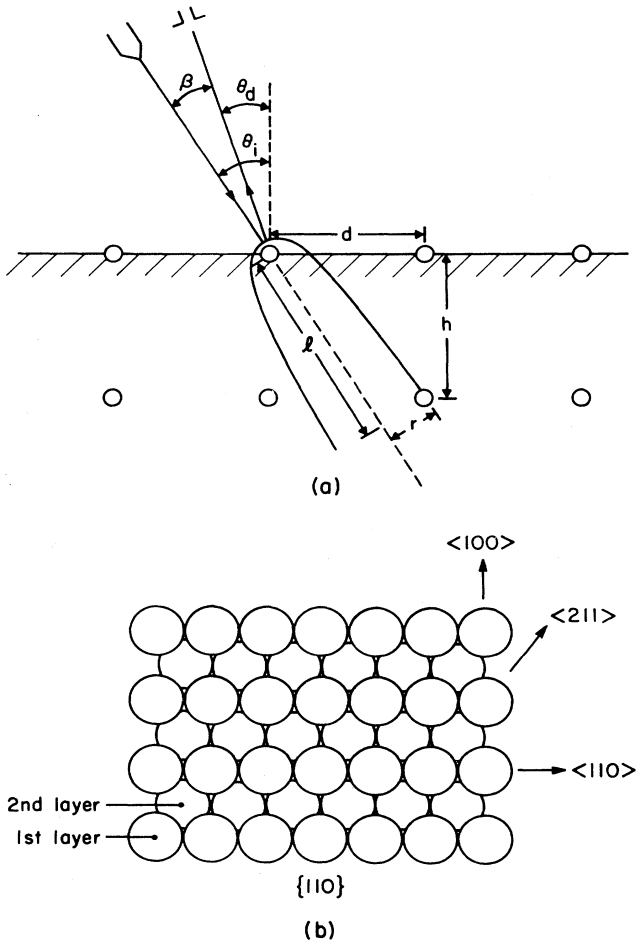

FIG. 1. Parameter definitions for the shadow-cone-enhanced desorption experiment. (a) The ion beam is incident at θ_i, the desorbed particles are detected at θ_d and $\beta=\theta_i-\theta_d$. The shadow cone is described by a radius r at a distance l behind the target atom. The d and h values describe the surface bond lengths. (b) The Ag{110} surface is characterized by troughs which are spaced by 4.086 Å and aligned with the ⟨110⟩ azimuth.

slightly different procedure was developed which involves a determination of the scaling factor from the known interatomic spacings of Ag. This procedure essentially allows us to use an experimentally determined shadow cone to examine an unknown structure. It will be discussed in detail in Sec. IV. A pair potential consisting of three parts was utilized to describe the interactions among silver surface atoms. The three parts are described by a repulsive Molière function for small internuclear separations ($r < 1.08$ Å), an attractive Morse potential ($D_e = 0.417$ eV, $r_e = 2.89$ Å, $\alpha = 1.41$ Å^{-1}) at long range ($r > 1.12$ Å), and a cubic spline to connect the two.[8]

For the three-dimensional calculations, the size of the model microcrystallite was tested independently at each angle of incidence for containment of the important dynamical events. In this study, a crystallite 4–6 atomic layers thick with a surface area of 80–100 atoms per layer is sufficiently large to contain all the significant desorption events without consideration of edge effects. The crystallites could be constructed using bond lengths appropriate for a bulk-terminated Ag{110} surface or for a surface which has relaxed according to various experimental observations. For example, the most recent high-energy ion-scattering studies suggest that the first-to-second-layer spacing is contracted by 9.5% and that the second-to-third-layer spacing is expanded by 6.0%.[2] For each set of initial conditions, approximately 350 different impact points were chosen which are uniformly distributed over a zone of irreducible surface symmetry. For each collision cascade that results in ejection of atoms from the surface, the initial conditions, final velocities, and the identities of the ejected particles may be stored for subsequent analysis. The polar angle distributions were plotted with a resolution of ±7° in the polar direction.

IV. RESULTS AND DISCUSSION

The polar angle distributions of the secondary ions desorbed from a Ag{110} surface bombarded at various angles of incidence by 2-keV Ar^+ ions are shown in Fig. 2. In all cases the data were obtained by keeping β fixed at 25°. In curve *a*, the secondary-ion intensity along the ⟨100⟩ azimuth, perpendicular to the ridges of the {110} face [Fig. 1(b)], exhibits a strong angular anisotropy with maximum intensities observed at $\theta_{ic} = 36.5°$ (i.e., $\theta_d = 11.5°$) and $\theta_{ic} = 68.0°$. With the crystal oriented along the ⟨110⟩ azimuth (curve *b*), parallel to the ridges of the {110} face, the intensity of Ag^+ ions exhibit local maxima at $\theta_{ic} = 29.5°$ and 60.0°. Along the ⟨211⟩ azimuth (curve *c*), the maximum peak intensities are detected at $\theta_{ic} = 31.5°$ and 70.0°.

In order to gain an initial level of understanding of the angular dependence of the observed secondary particle yield, two-dimensional computer simulations were performed using an unrelaxed lattice for 1-keV Ar^+-ion scattering in-plane from Ag{110} in the ⟨100⟩ direction. The results of these calculations are shown in Fig. 3, where the solid lines represent the trajectories of the incident ions during scattering from a variety of aiming points on the crystal surface. Clearly the impacts which are closer to an atom yield greater deflection of the incident particle. The net result, as shown in Fig. 3, is that the incident ions do not directly penetrate the region beneath the target atoms unless they are scattered in subsequent collisions. This forbidden envelope, often called the shadow cone, tilts as the angle of incidence increases.

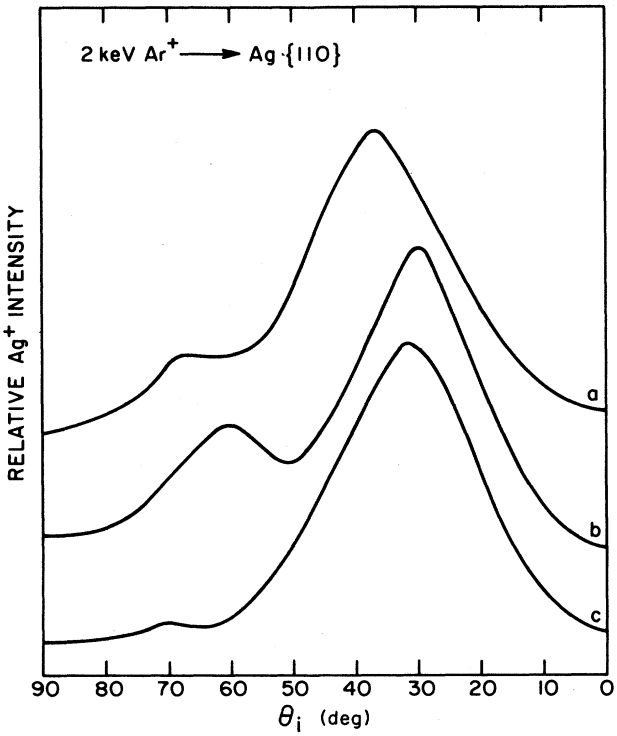

FIG. 2. The shadow-cone enhanced SIMS spectra of the desorbed Ag^+-ion yield as a function of the angle of incidence. The particles are collected along the (a) ⟨100⟩, (b) ⟨110⟩, and (c) ⟨211⟩ azimuth during 2-keV Ar^+-ion bombardment at a current of ~5 nA. Only particles desorbed in plane with $\beta = 25°$ are collected.

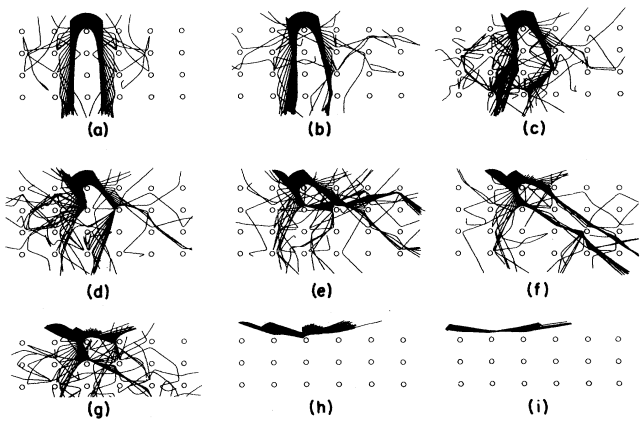

FIG. 3. Results from two-dimensional computer simulations of 1-keV Ar^+-ion scattering from the Ag{110} surface along the ⟨100⟩ azimuth. The high ion flux is observable at the tails of shadow cones. Note that one of the tails strongly interacts with second-layer atoms between $\theta_i = 30°$ and $\theta_i = 40°$. The angle of incidence θ_i is (a) 0°, (b) 10°, (c) 20°, (d) 30°, (e) 40°, (f) 50°, (g) 60°, (h) 70°, (i) 80°.

Note the concentration of incident ion flux along the shadow-cone edge. These simulations suggest that there are four types of interaction mechanisms which might result in the yield enhancement observed in our spectra. As shown schematically in Fig. 4, mechanisms F_1 and F_{2A} involve collisions with the ion flux at the forward edge of the shadow cone. These mechanisms as seen from Figs. 3(h) and 3(e), respectively, effectively induce a great deal of near-surface scattering and might be expected to enhance desorption. As we shall see, the peak at $\theta_{ic}=36.5°$ in Fig. 2(a) does, in fact, arise from mechanism F_{2A}, and the weaker peak observed at $\theta_{ic}=68°$ corresponds to desorption via mechanism F_1.

The importance of other shadow-cone-enhanced desorption processes is not completely obvious without examining many computer simulations such as those shown in Fig. 3 and obtained at various combinations of incident-ion kinetic energies and interatomic spacings. In general the B_{2A} mechanism shown in Fig. 4 is not important except at very high kinetic energy. At low kinetic energies, the shadow cone, as denoted in Fig. 3(g), becomes strongly distorted by neighboring atoms. The intensity of desorbed ions from the B_{2B} process is expected to rise to a peak for systems bombarded with high kinetic energy or small interatomic spacings. As seen in Figs. 3(d) and 3(e), this mechanism may strongly overlap with the F_{2A} process in our experimental condition.

To provide a more rigorous basis for our understanding of the secondary-ion angular anisotropy shown in Fig. 2, a series of three-dimensional molecular dynamics simulations of the desorption process were performed at incident angles between $\theta_i=15°$ and 90°, the results of which are shown in Fig. 5. The calculations not only provide a quantitative estimate of the yield of desorbed particles but also allow the microscopic dynamics to be closely evaluated.

These data are characterized by a main peak at $\theta_{ic}=25°$ with prominent shoulders at $\theta_{ic}=38°$ and 55°. A detailed analysis of individual trajectories associated with these peaks supports the mechanistic ideas developed from the two-dimensional computer simulations. The maximum observed at 25° is seen to arise primarily from collision cascades initiated by the strong interaction of the incident ions with second-layer atoms (mechanism F_{2A}) after the incident ions are focused by the shadow cones of first-layer atoms. These events are more effective in inducing desorption since they are initiated close to the surface. Similar considerations suggest that the peaks at 38° and 55° arise from cascades originating from the B_{2B} and F_{2A} mechanisms, respectively.

There are two factors which limit the general applicability of this theoretical approach for interpretation of spectra reported in this work. Most importantly, ~ 1000 individual trajectories are required for each angle of incidence to obtain statistically significant yields. Many weeks of computer time were needed to generate the data presented in Fig. 5. Further, to achieve containment of the dynamics at all angles, it is presently necessary to limit the incident kinetic energy to 500 eV or less. This value is below the lowest energy available to our experimental setup, so it is not yet possible to directly compare measured and calculated yields. The second, less significant factor is that the molecular-dynamics calculations provide predictions of the yield of neutral atoms rather than that of the experimentally measured ionized species. The yield of ionized species is believed to be reduced by a factor[19]

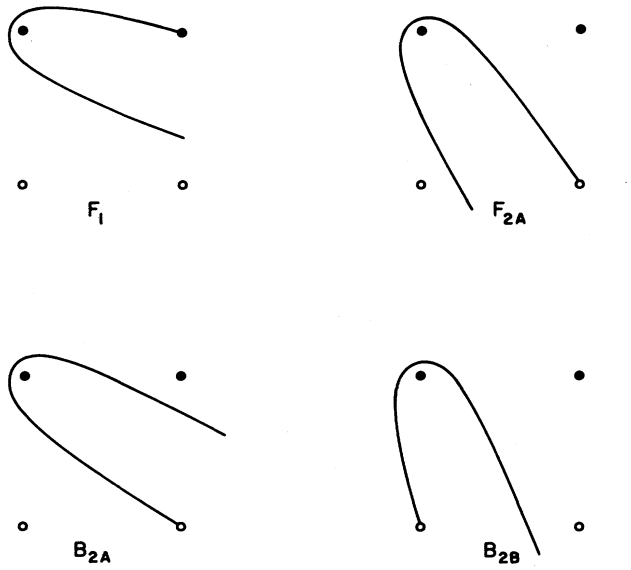

FIG. 4. The possible interaction mechanisms of the tails of the shadow cone with the top two layer atoms of the surface. The first-layer atoms are represented by filled circles, while the lower-layer atoms are represented by open circles. In general, the interaction mechanisms due to the left (backward) tail of the shadow cone do not contribute significantly to the SIMS yield enhancement.

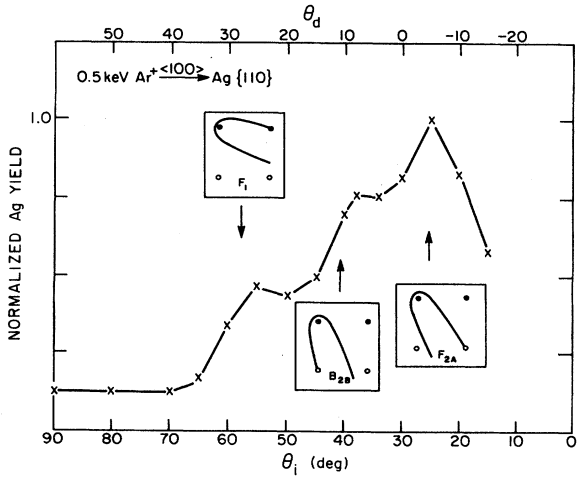

FIG. 5. Results from three-dimensional molecular-dynamics calculations of the Ag yield as a function of the angle of incidence. The Ar^+ primary energy is 500 eV and the Ag atoms are desorbed in plane along the ⟨100⟩ direction of the Ag{110} face. The calculated positions using the simple two-body potentials of the possible scattering mechanisms are shown as insets.

$$\exp\left[-\text{const}\times\frac{1}{v\cos\theta_d}\right], \quad (1)$$

where v is the velocity of an ion ejecting with takeoff angle θ_d. The trajectory of the ion may also be altered by the interaction of the ionic charge with its image in the substrate.[20] For values of θ_d between $\pm 45°$, neither of these effects are large enough to shift observed values of θ_{ic}, although the relative intensities of peaks may be altered somewhat. Application of Eq. (1) to the data of Fig. 5, for example, does not produce any measurable shifts in the peak positions. Further, we will show in the next section that the values of θ_{ic} are virtually independent of β which could not be possible if strong ionization effects were operative. In spite of the above difficulties, however, the full dynamical computer simulations do provide a valuable check for conclusions forthcoming from simpler theoretical approaches.

If shadow cones are indeed responsible for inducing the important angular features illustrated in Figs. 2 and 5, it should be possible to predict the position of these features using the shadow-cone shape followed by simple trigonometric arguments. The shape of the shadow cone as described by a shadow-cone radius r_s at a distance l behind the shadowing atom may be accurately calculated for the Thomas-Fermi Molière potential using established procedures.[15] These calculations may be completed in a fraction of a second on the most primitive personal computer. The critical values of θ_i for the important scattering mechanisms are superimposed on the three-dimensional computer-calculated yields in Fig. 5. Note the excellent agreement between the two methods of calculation. For this particular example, then, the important peaks in the angular distributions can accurately be predicted from simple shadow-cone arguments.

Our next challenge is to provide a detailed analysis of the data shown in Fig. 2 using the simple shadow-cone calculation. These data are particularly important since they are reported for a variety of azimuths, allowing different combinations of d, the interatomic spacing, and h, the interplanar spacing, to be tested. The experimental and calculated θ_{ic} values are summarized in Table I.

The calculated values depend to some degree on the scaling factor a, applied to the Firsov screening length. Up to this point, we have arbitrarily chosen a value of 1.0 for this factor, since little is known about what number to choose for the Ar/Ag mass combination. From our data, however, it is possible to determine the optimal value for a and to independently determine h. For Ag{110}, LEED data provides conclusive evidence that the surface atoms are not laterally displaced.[21] Thus, it is possible to examine the θ_{ic} value associated with the three F_1 scattering mechanisms using known values of d. The deviations between calculated and measured angles are then minimized by varying a. This fitting procedure provides a result which is then independent of any inward or outward relaxation of surface planes. With a known, it is then possible to determine h from the F_{2A} mechanisms. Along ⟨100⟩, F_{2A} provides information about the first- and third-layer spacing, h_{13}. Along ⟨211⟩, F_{2A} is sensitive to the first- and second-layer spacing, h_{12}. The F_{2A} mechanism along the ⟨110⟩ direction is not easily interpretable due to distortion effects discussed further below. From this analysis, then, we find that $a=1.03$, $h_{12}=2.770$ Å (bulk 2.889 Å), and $h_{23}=1.332$ Å (bulk 1.445 Å). It is possible to estimate errors from the experimental reproducibility of $\pm 0.5°$ in θ_{ic} determinations. For this case, h_{12} is relaxed inward by $(7.8\pm 2.5)\%$ and h_{13} is relaxed by $(4.1\pm 2.1)\%$. These values are in excellent agreement with recent studies of the surface reconstruction of Ag{110}.[2,3] Note also that the calculated value for a is in excellent agreement with empirical methods used to estimate the value of this parameter.[18]

As discussed above, and as is evident from Table I, the computed θ_{ic} for F_{2A} along ⟨110⟩ occurs about 6° closer to the normal than is observed experimentally. The two-dimensional computer simulations suggest that the shadow cones are significantly distorted by the presence of nearby atoms along this rather densely packed azimuth. The effect is illustrated in Fig. 6(a) where the shadow-cone shapes are computed using simple two-body interactions and the full dynamics formalism. Note that the distortion becomes more significant as the incident particle penetrates deeper into the solid. These difficulties are not

TABLE I. Experimental and calculated values of θ_{ic}.

Azimuth	d (Å)[a]	h (Å)[a]	Shadow-cone mechanism	θ_{ic} (deg) experiment[b]	θ_{ic} (deg) calculation[c] I	II
⟨100⟩	4.086	0	F_1	68.0	67.4	67.4
	4.086	2.770	F_{2A}	36.5	36.5	35.6
⟨110⟩	2.889	0	F_1	60.0	60.0	60.0
	2.889	2.770	F_{2A}	29.5	23.2	22.4
⟨211⟩	5.005	0	F_1	70.0	70.8	70.8
	2.502	1.332	F_{2A}	31.5	31.5	30.0

[a]The interatomic distance (d) and the interplanar spacing (h) are defined in Fig. 1. The values for h are determined using the method described in the text. The values given for d are bulk values.

[b]Values determined from the data in Fig. 2 are taken for 2000-eV Ar^+ ions incident on Ag{110} with $\beta=25°$.

[c]Calculated values from the shadow-cone shape assuming (I) relaxed lattice and (II) unrelaxed lattice, assuming a scaling factor for the Firsov screening length of 1.03. See text for further description.

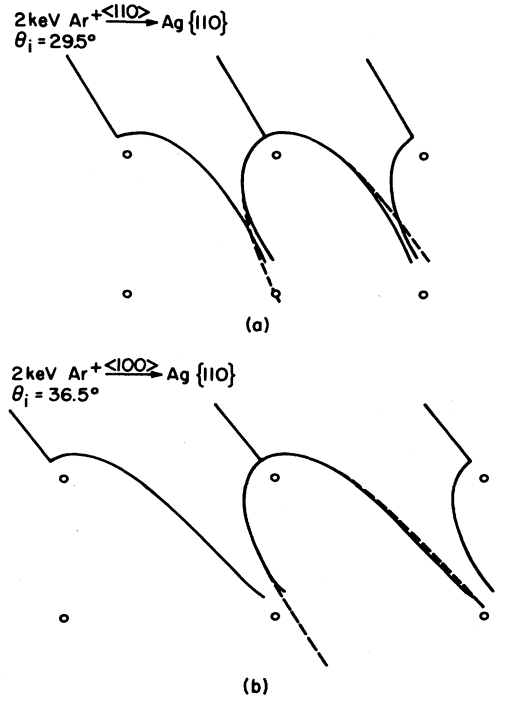

FIG. 6. Illustration of the distortion of the shape of the shadow cone beneath the surface layer. The dotted lines represent the shape of the shadow cone calculated from the two-body interaction model. The solid lines represent results from the full dynamics interaction model.

present along ⟨100⟩ as shown in Fig. 6(b) nor along ⟨211⟩ since the interatomic spacings are rather large relative to the shadow-cone radius. It is expected that distortion efforts might also be minimized by increasing the kinetic energy of the incident ion.

At this stage, we believe that the important features of the angular anisotropies are well understood and can even be utilized to determine bond lengths. There are several additional experimental configurations which are important to further verify our model and which may lead to additional applications. Of major importance is to evaluate the significance of the value of β, the angle between the detector and the incident ion beam. If these anisotropies are truly due to enhanced desorption yields initiated by collision cascades and not due to ionization artifacts, the angular features must be independent of β. As shown in Fig. 7 for 2-keV Ar^+ ions incident upon ⟨110⟩, this condition is observed to hold quite well even for the F_{2A} peak, whose shadow cone is known to be strongly distorted. The changes in the relative intensity of the F_1 peak to the F_{2A} peak as a function of β arise from a blocking of desorbing atoms by other surface atoms, which occurs only at large values of θ_i and small values of β. The β independence of θ_{ic} is observed at all azimuths and all combinations of θ_i and β except at large values of θ_d ($=\theta_i-\beta$). In this case it is possible that the strong bending force exerted on ejecting ions by the image potential may be responsible for the small observed shifts. The measured value of θ_{ic} has also been found to be independent of the kinetic energy of the secondary ions over the range of 2–20 eV and of the target temperature between 300 and 700 K

The determination of the dependence of θ_{ic} on β may prove to be important in the analysis of more complex surfaces. As we know from the computer simulations[12] nearly 95% of the desorbed material arises from the top atomic layer. This result suggests that overlayer atoms may strongly influence the trajectories of atoms below the surface. If a small fraction of the Ag atoms are covered by an adsorbate of different mass, the desorbing Ag atoms will be deflected by channeling or blocking of these overlayer atoms. We illustrate this point in a preliminary fashion in Fig. 8, where the Ag{110} surface has been exposed to a high does of Cl_2. Note that the θ_{ic} value is now a strong function of β, as seen in Fig. 8(a). When the same data are plotted as a function of θ_d, as shown in Fig. 8(b), however, the peak intensities appear at the same angle even though θ_i is changing. This result indicates that the Cl overlayer is controlling the trajectory of the desorbing Ag species. The θ_{ic} value associated with the Cl-ion intensity, however, continues to exhibit β independence.[22] This type of observation may become an important new method for distinguishing first- and second-layer atoms.

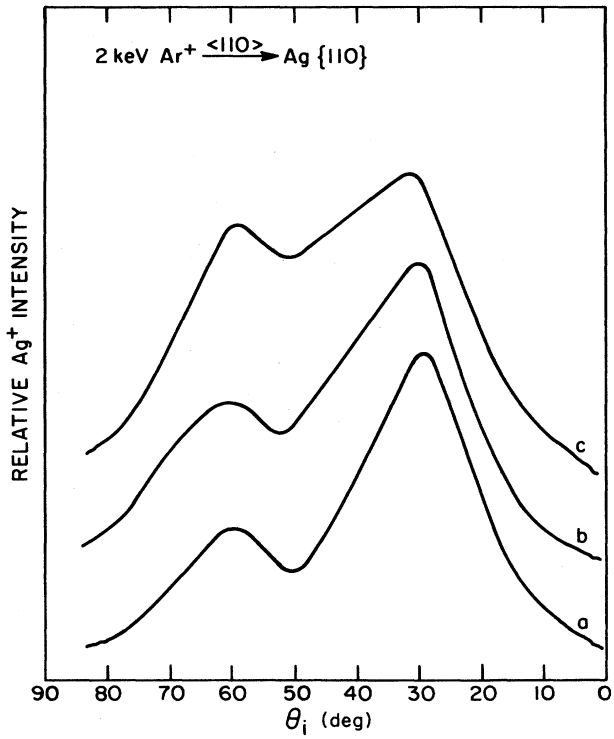

FIG. 7. Experimental polar angle distributions for (a) $\beta=25°$, (b) $\beta=30°$, and (c) $\beta=40°$. The peaks at $\theta_{ic}\simeq 29.5°$ and $\theta_{ic}=60.0°$ arise from the interaction of the forward tail of the shadow cone with the second- and first-layer atoms of the Ag{110} surface, respectively.

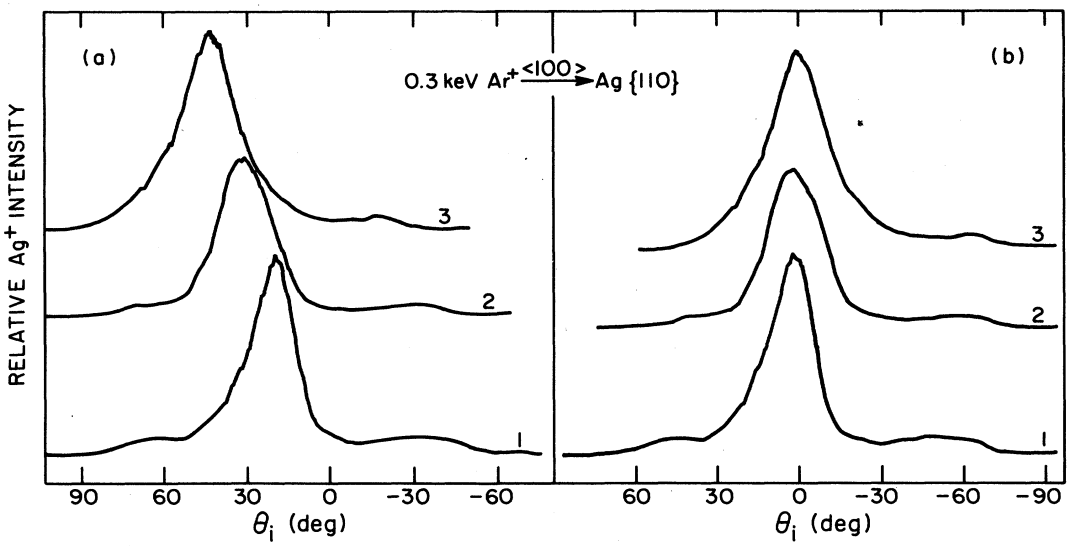

FIG. 8. Experimental polar angle distributions of the ejected Ag^+ ions from Ag{110} exposed to 8 L of Cl_2 (approximately one layer). In (a) the Ag^+-ion intensity is plotted as a function of θ_i while in (b) the Ag^+-ion intensity is measured as a function of θ_d. For curve 1, $\beta=18°$; for curve 2, $\beta=30°$; and for curve 3, $\beta=45°$.

V. CONCLUSIONS AND PROSPECTS

In this work, we have observed that the desorption yield of single-crystal surfaces bombarded by keV incident ions is significantly enhanced when the shadow-cone edges intersect surface or near-surface atoms. This observation has been supported by several theoretical models including a very simple two-body collision model derived from analogous ion-scattering experiments. It is quite remarkable to us that such a complex process as ion-beam-induced desorption is describable by such a simple formalism. We are aware that the ideas developed in this paper are not totally unrelated to the ideas of lattice transparency that were developed during the late 1960s.[23] It is most encouraging, however, that our approach offers the possibility of learning a great deal about the structure of rather complex surfaces.

There are a number of significant potential advantages of our approach that should complement other ion-scattering methods utilizing shadow-cone concepts. First, and perhaps most importantly, the secondary-ion angular anisotropy is only a function of θ_i. Except under special conditions, blocking and channeling of the outgoing particles are not significant. This means that the secondary particles may be detected at any (or all) angles, allowed for extremely simple experimental designs. Secondly, the detection sensitivity is potentially very high, especially for those cases where the desorbed species is characterized by a large ionization probability. There are, in general, many orders of magnitude more particles desorbed than in analogous ICISS experiments. Thirdly, the high sensitivity allows experiments to be performed using extremely low ion doses to avoid surface damage and to study dilute concentrations of adsorbates on surfaces. In preliminary experiments, for example, we have already been able to examine very low coverages of Cl adsorbed on Ag{110}, a regime where dipole-dipole interactions between overlayer atoms are minimized.[24]

The shadow-cone radii employed in these experiments are quite large relative to the interatomic spacings of Ag. This set of conditions produces the annoying distortion effects noted for atoms below the surface along close-packed directions. It will be interesting to test our approach using incident ions of other masses and kinetic energies to see if these effects can be eliminated. Finally, it has already been noted that our approach is particularly valuable for studying covalent solids such as GaAs. These lattices are much less susceptible to distortion due to their large interatomic spacings. For example, shadow-cone-enhanced desorption experiments have successfully determined the chain rotation angle in GaAs{110} reconstructed surfaces.[25]

ACKNOWLEDGMENTS

The authors wish to thank Rik Blumenthal, R. S. Williams, and B. J. Garrison for many helpful discussions concerning this work. The National Science Foundation, The Office of Naval Research, the IBM Corporation, and the Donors of The Petroleum Research Fund, administered by the American Chemical Society, provided partial financial support.

*Permanent address: Department of Chemistry, University of Hawaii at Manoa, 2545 The Mall, Honolulu, HI 96822.

[1]J. F. Van der Veen, Surf. Sci. Rep. **5**, 199 (1985).
[2]E. Holub-Krappe, K. Horn, J. W. M. Frenken, R. L. Kraus, and J. F. Van der Veen, Surf. Sci. **188**, 335 (1987).
[3]Y. Kuk and L. C. Feldman, Phys. Rev. B **30**, 5811 (1984).
[4]M. Aono, C. Oshima, S. Zaima, S. Otani, and Y. Ishizawa, Jpn. J. Appl. Phys. **20**, L829 (1981).

[5]M. Aono, Y. Hou, R. Souda, C. Oshima, S. Otani, and Y. Ishizawa, Phys. Rev. Lett. **50**, 1293 (1983).
[6]J. A. Yarmoff, D. M. Cyr, J. H. Huang, S. Kim, and R. S. Williams, Phys. Rev. B **33**, 3856 (1986).
[7]R. Souda, M. Aono, C. Oshima, S. Otani, and Y. Ishizawa, Surf. Sci. **128**, L236 (1983).
[8]N. Winograd, Prog. Solid State Chem. **13**, 285 (1982).
[9]J. Singh, C. T. Reimann, J. P. Baxter, G. A. Schick, P. H. Kobrin, B. J. Garrison, and N. Winograd, J. Vac. Sci. Technol. A **5**, 1191 (1987).
[10]R. A. Gibbs and N. Winograd, Rev. Sci. Instrum. **52**, 1148 (1981).
[11]B. J. Garrison, N. Winograd, and D. E. Harrison, Jr., Phys. Rev. B **18**, 6000 (1978).
[12]N. Winograd, D. E. Harrison, Jr., and B. J. Garrison, Surf. Sci. **78**, 467 (1978).
[13]I. M. Torrens, *Interatomic Potentials* (Academic, New York, 1972).
[14]T. M. Buck, I. Stensgaard, G. H. Wheatley, and L. Marchut, Nucl. Instrum. Methods **170**, 519 (1980).
[15]J. A. Yarmoff and R. S. Williams, Surf. Sci. **127**, 461 (1983).
[16]S. H. Overbury and D. R. Huntley, Phys. Rev. B **32**, 6278 (1985).
[17]B. Poelsema, L. K. Verhey, and A. L. Beers, Surf. Sci. **64**, 554 (1977).
[18]D. J. O'Conner and R. J. MacDonald, Radiat. Eff. **34**, 247 (1977).
[19]M. L. Yu, Phys. Rev. Lett. **47**, 1325 (1981).
[20]R. A. Gibbs, S. P. Holland, K. E. Foley, B. J. Garrison, and N. Winograd, J. Chem. Phys. **76**, 684 (1982).
[21]M. Maglietta, E. Zanazzi, F. Jona, D. W. Jepsen, and P. M. Marcus, J. Phys. 3287 (1977).
[22]C. C. Chang and N. Winograd (unpublished).
[23]See, for example, G. Carter and J. S. Colligan, *Ion Bombardment of Solids* (American Elsevier, New York, 1968).
[24]C. C. Chang, G. Malafsky, and N. Winograd, J. Vac. Sci. Technol. A **5**, 981 (1987).
[25]R. Blumenthal, S. K. Donner, J. L. Herman, R. Trehan, K. P. Caffey, E. Furman, N. Winograd, and B. D. Weaver, J. Vac. Sci. Technol. B **6**, 1444 (1988).